Inorganic Chemistry

pubs.acs.org/IC
Article

Mixed Metal Amide-Hydride Solid Solutions for Potential Energy Storage Applications

Thi Thu Le,* Simone Bordignon, Michele R. Chierotti, Yuanyuan Shang, Alexander Schökel, Thomas Klassen, and Claudio Pistidda*

Cite This: *Inorg. Chem.* 2024, 63, 11233−11241

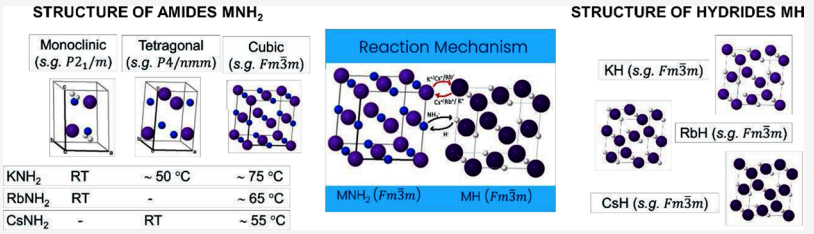

ABSTRACT: Mixed solid solutions have played an important role in improving the kinetics and performance of hydrogen storage materials, as reported for the Li−Mg−N−H, K−Mg−N−H, and Rb−Mg−N−H systems. Besides, the formation of a homogeneous solid solution, mostly due to partial ionic substitution, is known to be an effective approach to improve the ionic conductivity of a material, which is an important property in electrochemical applications. We have reported a series of solid solutions based on mixed amide-hydride materials of the Group 1 elements, e.g., $K(NH_2)_xH_{1-x}$, $Rb(NH_2)_xH_{1-x}$, and $Cs(NH_2)_xH_{1-x}$, via the exchange of NH_2^-/H^- anions with the change of the lattice cell of the solid solution. Extending the research in this direction, we study the M−N−H solid solution in the MNH_2−MH systems (M = K, Rb, Cs, and their combinations), i.e., KNH_2−RbH, $RbNH_2$−KH, $RbNH_2$−CsH, and $CsNH_2$−RbH via ex situ/in situ XRD, IR, and ^{1}H 2D solid-state NMR. The results obtained confirm the formation of mixed metal amide-hydride solid solutions associated with an exchange between both anionic (NH_2^- and H^-) and cationic species (K^+, Rb^+, and Cs^+). With this study, we aim to create an accessible library of M−N−H solid solutions for further studies as additives for hydrogen storage materials or ionic conductors.

1. INTRODUCTION

Metal amide-hydride materials have been extensively investigated in recent years for use in energy storage applications and specifically for storage applications in hydrogen technology (e.g., $LiNH_2$-LiH,[1−6] $Mg(NH_2)_2$-2LiH,[7−14] $Mg(NH_2)_2$-KH,[15] and $Mg(NH_2)_2$-RbH[16]) and as solid electrolytes[17−19] for all solid-state batteries. In hydrogen storage applications, amide-hydride systems prove promising candidates especially due to their high hydrogen storage capacity and tunable thermodynamics, which allows hydrogen desorption/absorption to occur at temperatures below 150 °C.[20] However, the sluggish desorption/absorption kinetics of these amide-hydride systems limit their potential employment in commercial applications. In such cases, metal hydrides-based additives such as KH, RbH, and CsH can effectively improve the hydrogen sorption kinetics and alter the thermodynamics of amide-hydride systems, in particular of $Mg(NH_2)_2$-2LiH.[21−25] These metal hydrides promote the formation of intermediate phases/solid solutions, which reduce the kinetic barrier of the amide/hydride interfacial reaction and lower the operating temperature of the Li−Mg−N−H system. Other solid solutions, such as the Li−N−H ones (e.g., $Li_{2+x}(NH)_{1-x}N_xH_x$ and $Li_{2+x}NH$), were synthesized to modify the thermal stability and ammonia reactivity of the LiNH-LiH system,[6] while Ca_2NH−Ca_2N solid solutions were studied as catalysts to promote low-temperature ammonia synthesis.[26] In general, solid solutions are not only important for hydrogen storage but also for the ionic conduction of complex metal hydrides. The formation of a homogeneous solid solution by ion mixing is one of the most common ways to improve the ionic conductivity of a material,[27] most likely due to the structural perturbations or modifications that facilitate the migration of ions, as observed in the $LiBH_4$−LiX (X = Cl^-, Br^-, and I^-)[28,29] and $NaBH_4$−NaI.[30]

Our previous studies reported the formation of mixed amide-hydride solid solutions, such as $K(NH_2)_xH_{1-x}$, $Rb(NH_2)_xH_{1-x}$, and $Cs(NH_2)_xH_{1-x}$, via the exchange of anionic species (NH_2^- in amides and H^- in hydrides) for the KNH_2−KH,[31] $RbNH_2$−RbH,[16] and $CsNH_2$−CsH[32] systems using

Received: March 12, 2024
Revised: May 13, 2024
Accepted: May 16, 2024
Published: May 30, 2024

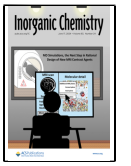

https://doi.org/10.1021/acs.inorgchem.4c01016
Inorg. Chem. 2024, 63, 11233−11241

both experimental determinations and theoretical calculations. The relative amides (i.e., KNH_2, $RbNH_2$, and $CsNH_2$) undergo a structural transition from monoclinic space group (s.g.) $P2_1/m$ (for both KNH_2 and $RbNH_2$) and tetragonal s.g. $P4/nmm$ (for $CsNH_2$) to cubic crystal structures with the same s.g. $Fm\bar{3}m$ within the temperature range of 50−80 °C. On the contrary, the corresponding hydrides, namely, KH, RbH, and CsH, have similar cubic crystal structures (s.g. $Fm\bar{3}m$), which remain unchanged upon temperature variation. Furthermore, the dissolution of NH_2^- into the KH (or RbH and CsH) hydride structure leads to the structural expansion of the $M(NH_2)_xH_{1-x}$ solid solutions (M = K, Rb, and Cs). This change in the lattice structure could lead to significant changes in the material's functional properties, such as ionic conductivity, similarly to what observed in ionic conducting systems like $LiBH_4$−LiX (X = Cl^-, Br^-, and I^-)[28,29] and $NaBH_4$−NaI.[30] In particular, KNH_2 exhibits an ionic conductivity of 3.56×10^{-4} S cm^{-1} at 150 °C, which can be further enhanced by introducing structural disorder.[18] These findings suggest a high potential for the application of these amide-hydride solid solutions (with modified structures) in the energy storage field. In this work, we report the formation of solid solutions in the MNH_2−MH system, namely, KNH_2−RbH, $RbNH_2$−KH, $CsNH_2$−RbH, and $RbNH_2$−CsH, via the exchange of anion and cation species. It is well-known that several factors determine the limits of solubility. These are expressed as a series of rules, the so-called William Hume−Rothery Rules: (i) atomic size factor (extensive substitutional solid solution occurs only if the relative difference between the atomic radii of the two species is less than 15%); (ii) crystal structures of the two elements must be identical; (iii) two species (the solute and the solvent atoms) should typically have the same valence; and (iv) electronegativity difference was close to 0. In the present study, there are clear structural analogies among these MNH_2 amides and between them and the MH hydrides. Moreover, comparing the relative difference between the size of K^+ (r_{ion} = 1.52 Å), Rb^+ (r_{ion} = 1.66 Å), and Cs^+ (r_{ion}= 1.81 Å) cations and between the size of NH_2^- (r_{ion} = 1.73 Å) and H^- (r_{ion} = 1.53 Å) anions, the radii difference for any of their combinations is less than 15%, which, according to the Hume−Rothery rules, allows for the formation of $M(NH_2)_xH_{1-x}$ solid solutions, based on the substitution of both anion and cation species. The proposed diagram for ion substitutions in these systems is illustrated in Figure 1. As mentioned above, ionic hydrides (KH, RbH, and CsH) have been shown to be effective additives to improve the kinetic and thermodynamic properties of the most promising amide-hydride hydrogen storage system, $Mg(NH_2)_2$-2LiH. Therefore, the use of such mixed metal amide-hydride as additives in the hydrogen storage systems might be possible. Moreover, the formation of solid solutions displaying crystal lattice disorder (due to the different ionic radius of exchanged cations and anions) could create channels for ion diffusion and therefore increase the ionic conduction within the solid lattice, highlighting the potential use of these alkali metal mixed amide-hydride solid solutions for further studies on the ionic conductivity or as dopants/catalysts for hydrogen storage materials.

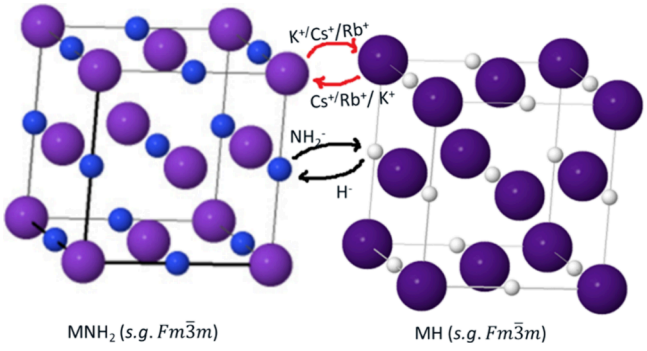

Figure 1. Schematic diagram of the amide-hydride reaction mechanism.

2. EXPERIMENTAL METHOD

2.1. Materials Preparation. Potassium hydride (KH) in paraffin was purchased commercially (35.8 wt % KH purity, Sigma-Aldrich). The synthesis of potassium amide (KNH_2), rubidium amide ($RbNH_2$), rubidium hydride (RbH), cesium hydride (CsH), and cesium amide ($CsNH_2$) followed the same procedures, as reported in refs 16 and 31. KNH_2 was synthesized by repeated ball-milling of the potassium hydride in a Pulverisette planetary mill at 500 rpm with a ball-to-powder ratio (BPR) of 20:1 under 7 bar of NH_3 for 5 h. This process was repeated four times for a total milling time of 20 h. Between each repetition, the high-pressure vessel was evacuated and refilled with fresh NH_3. RbH was synthesized by ball-milling metallic rubidium (Rb 99.8%, Alfa Aesar) in 50 bar of H_2 at 500 rpm for 13 h with a BPR of 60:1, followed by further annealing at 180 °C for 5 h under 70 bar of H_2. $RbNH_2$ was synthesized by heat treatment of metallic Rb in 7 bar of NH_3 at 250 °C for 13 h. The mixtures $x$$KNH_2$ + $(1 - x)$RbH and $x$$RbNH_2$ + $(1 - x)$KH with x = {0, 0.5, 0.7, 1} were prepared by hand-grinding using an agate mortar followed by heat treatment at 270 °C for 3 h. To avoid oxidation of the materials, all samples were prepared under a protective atmosphere in a continuous Ar-filled glovebox (MBraun, Germany) with an oxygen and humidity concentration of less than 1 ppm.

2.2. Materials Characterization. Ex situ powder X-ray diffraction (XRD) experiments were performed using a D8 Discover diffractometer (Bruker AXS GmbH, Karlsruhe, Germany) equipped with a Cu Kα beam (λ = 1.54184 Å) and 2D VANTEC detector. The diffractograms were acquired in the 2θ range from 10° to 90°, in nine steps with an exposure time of 400 s per step. A small amount of the sample was placed on a flat commercial sample holder and sealed with an airtight poly(methyl methacrylate) lid to prevent oxidation.

In situ synchrotron powder X-ray diffraction (in situ SR-PXD) measurements were performed at the Powder Diffraction and Total Scattering Beamline (P02.1) of Petra III (Desy Hamburg, Germany)[33] using a monochromatic X-ray beam (λ = 0.20734 Å). The diffraction patterns were collected by a Varex4343CT detector with an array of 2880 × 2880 pixels and a pixel size of 150 μm × 150 μm with an exposure time of 10 s per pattern. Samples were loaded into sapphire capillaries under a purified Ar atmosphere and then mounted on an in-house developed in situ cell, in which operating temperatures and pressures can be controlled.[34,35] The measurements for all mixtures were carried out under 1 bar of Ar, with the sample heated up from room temperature (RT) to 270 °C at a heating rate of 5−10 °C/min, held isothermally at 270 °C for 30 min, and then cooled down to RT. A small difference in the measurement conditions of the starting materials (KNH_2, RbH, $RbNH_2$, and KH) is that they were kept isothermally at 270 °C for 10 min instead of 30 min. The 2D diffraction images were integrated into 1D diffractograms using the Fit2d software, and the quantitative analyses were performed using the Rietveld refinement method with the Material Analysis Using Diffraction software (MAUD).[36] Structural information on known phases was obtained from the International Crystal Structure Database (ICSD) using the ICSD-Desktop software.

The pure and mixed samples were characterized using the Fourier transform infrared spectroscopy (Cary 630 FT-IR spectrometer, Agilent Technologies Deutschland GmbH, Waldbronn, Germany). The FT-IR spectrometer was placed in an Ar-circulated glovebox with

https://doi.org/10.1021/acs.inorgchem.4c01016
Inorg. Chem. 2024, 63, 11233−11241

oxygen and moisture concentrations below 5 ppm. The background was calibrated for each measurement; a small amount of material was placed on the diamond ATR top plate, and the FT-IR spectrum was acquired at RT in a full frequency range of 4000−650 cm^{-1} with a spectral resolution of 4 cm^{-1} and a number of scans of 300.

Solid-state nuclear magnetic resonance (SSNMR) experiments were run on a Jeol ECZR 600 instrument, operating at a frequency of 600.13 MHz for ^1H and equipped with a 3.2 mm probe. Rotors were packed inside a glovebox to prevent sample decomposition. The ^1H MAS spectra were acquired at probe temperature at a spinning speed of 20 kHz (4 scans; optimized relaxation delays equal to 200 or 280 s, corresponding to $5{\cdot}T_1$ for quantitative measurements). The 2D ^1H double-quantum (DQ) MAS experiments were performed at probe temperature at a spinning speed of 20 kHz with the back-to-back (BABA)-xy16 recoupling pulse sequence with excitation time durations of eight rotor periods (^1H 90° = 2.2 μs; 4 scans; $t1$ increments = 64; relaxation delay = 50 or 72 s, corresponding to $1.27{\cdot}T_1$). The ^1H chemical shift scale was calibrated with adamantane (^1H signal at 1.87 ppm with respect to primary standard tetramethylsilane) as an external standard.

3. RESULTS AND DISCUSSION

3.1. KNH_2−RbH System. Figure 2 shows the room temperature XRD patterns of the annealed $x KNH_2 + (1 - x)$RbH samples, where x = {0, 0.5, 0.7, 1}. Note that in the XRD pattern of the compositions featuring x = {0.5, 0.7}, the reflections of KNH_2 (monoclinic, s.g. $P2_1/m$, labeled ♏) are not visible. This indicates that KNH_2 reacted with RbH, accompanied by the formation of a single cubic phase (♣, s.g. $Fm\bar{3}m$). In addition, the metallic K (labeled ϕ) and an unknown phase (labeled ?) are also present. This may indicate a partial decomposition of reactants under given conditions. In addition, for the x = 0.5 composition, the peaks appear broadened, particularly at the high Q-values, suggesting an overlap of multiple phases due to incomplete reactions between the amide and hydride. To clarify these, in situ SR-PXD measurements were carried out.

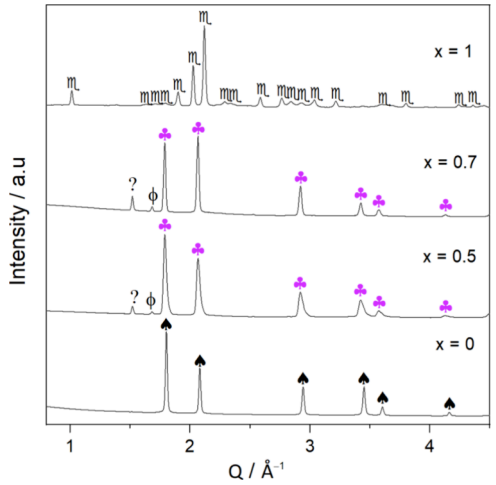

Figure 2. RT XRD of the annealed $x KNH_2 + (1 - x)$RbH samples, with x = {0, 0.5, 0.7, 1}. ♣ = Rb−K−N−H solid solution ($Fm\bar{3}m$), ♏ = KNH_2 ($P2_1/m$), ♠ = RbH ($Fm\bar{3}m$), ϕ = K metallic ($Im\bar{3}m$), and ? = unknown phase.

In order to assess the formation of the single cubic phase seen in Figure 2, as well as the microstructural evolution of the investigated material under temperature and pressure variations, in situ SR-PXD experiments were carried out on the initial and mixed samples. Figure 3 shows the in situ SR-PXD data of the $x KNH_2 + (1 - x)$RbH samples, where x = {0, 0.5, 0.7, 1}. As can be seen in Figure 3, the in situ SR-PXD data of the KNH_2 starting material show two phase transitions: the first one corresponds to the phase transformation of KNH_2 from a monoclinic (s.g. $P2_1/m$) to a tetragonal structure (s.g. $P4/nmm$, ♦) at about 55 °C and the second one is the phase conversion of KNH_2 from the tetragonal (s.g. $P4/nmm$) to the cubic (s.g. $Fm\bar{3}m$, ♥) structure at about 75 °C, while RbH (s.g. $Fm\bar{3}m$, ♠) does not undergo structural changes during the heating and cooling periods. These observations agree with those reported in references and literatures.[16,31] For mixed samples with x = {0.5, 0.7}, their in situ SR-PXD data appear similar, and both differ from the in situ SR-PXD data of the starting samples (KNH_2 and RbH). At the beginning of the heating period, both x = 0.5 and x = 0.7 mixtures show the existence of monoclinic KNH_2 (♏), cubic RbH (♠). Besides, tiny peaks of metallic K (ϕ) and unknown phase (?) are also detected. Trying to understand the reason for the presence of metallic K and the unknown phase found for the mixed samples, the gas evolution for the x = 0.7 composition during the mixing under inert atmosphere of KNH_2 and RbH was monitored by mass spectrometer (MS). As demonstrated in ESI-Figure S1, the investigation's findings indicated signs of hydrogen and ammonia release during mixing. The presence of metallic K and an unknown phase, along with the gas evolution found by MS, indicates a partial decomposition of reactants. However, according to the Rietveld refinement, the cell parameter of the RbH-like structure for the x = 0.7 composition (ESI-Figure S2), a, is 6.0405617 Å, thus larger than the RbH cell parameter (a = 6.0363336 Å) of the pure sample (ESI-Figure S3). This increase corresponds to a volume expansion of RbH of 0.21%. This supports the assumption that the solid solution formation by the cation and anion substitution, which underlies the interaction between KNH_2 and RbH, already occurred during grinding. As the temperature increases, phase transitions are found for KNH_2 from the monoclinic (♏) to the tetragonal (♦) and then to the cubic (♥) structure, as predicted, while the RbH peaks (♠) remain unchanged, like what was observed for the pure KNH_2 and RbH samples. At $T \sim 160$ °C, solid solution formation begins, corresponding to the disappearance of the cubic KNH_2 diffraction peaks and the shift of the cubic RbH peaks toward the lower Q values, indicating a gradual transformation from the RbH to the solid solution structure. This process continues during the heating period and is completed at 270 °C, with the observation of a complete single cubic solid solution phase (s.g. $Fm\bar{3}m$, ♣). This phase (♣) is stable on cooling and at RT after the measurement. No Bragg peaks of initial materials (i.e., monoclinic KNH_2 and cubic RbH) are detected, suggesting the stability of the solid solution. In addition, small peaks of elemental K (ϕ) and unknown phase (?) are back at RT after the measurement for both x = 0.5 and x = 0.7 compositions, like what was observed in the ex situ XRD (see Figure 2).

3.2. $RbNH_2$−KH System. Similarly, the room temperature XRD diffractograms of the $x RbNH_2 + (1 - x)$KH samples after being annealing at 270 °C are shown in Figure 4. The data show that for the compositions x = {0.5, 0.7}, the Bragg peaks of the $RbNH_2$ (ψ) and KH (δ) phases are not detected, but instead, a single cubic phase (♣, s.g. $Fm\bar{3}m$) is observed, indicating the dissolution of $RbNH_2$ and KH within the structure. Small peaks related to elemental K (ϕ) and an unknown phase (?) are also observed, similarly to the KNH_2−RbH system (Section 3.1). It should be noted that peak

https://doi.org/10.1021/acs.inorgchem.4c01016
Inorg. Chem. 2024, 63, 11233−11241

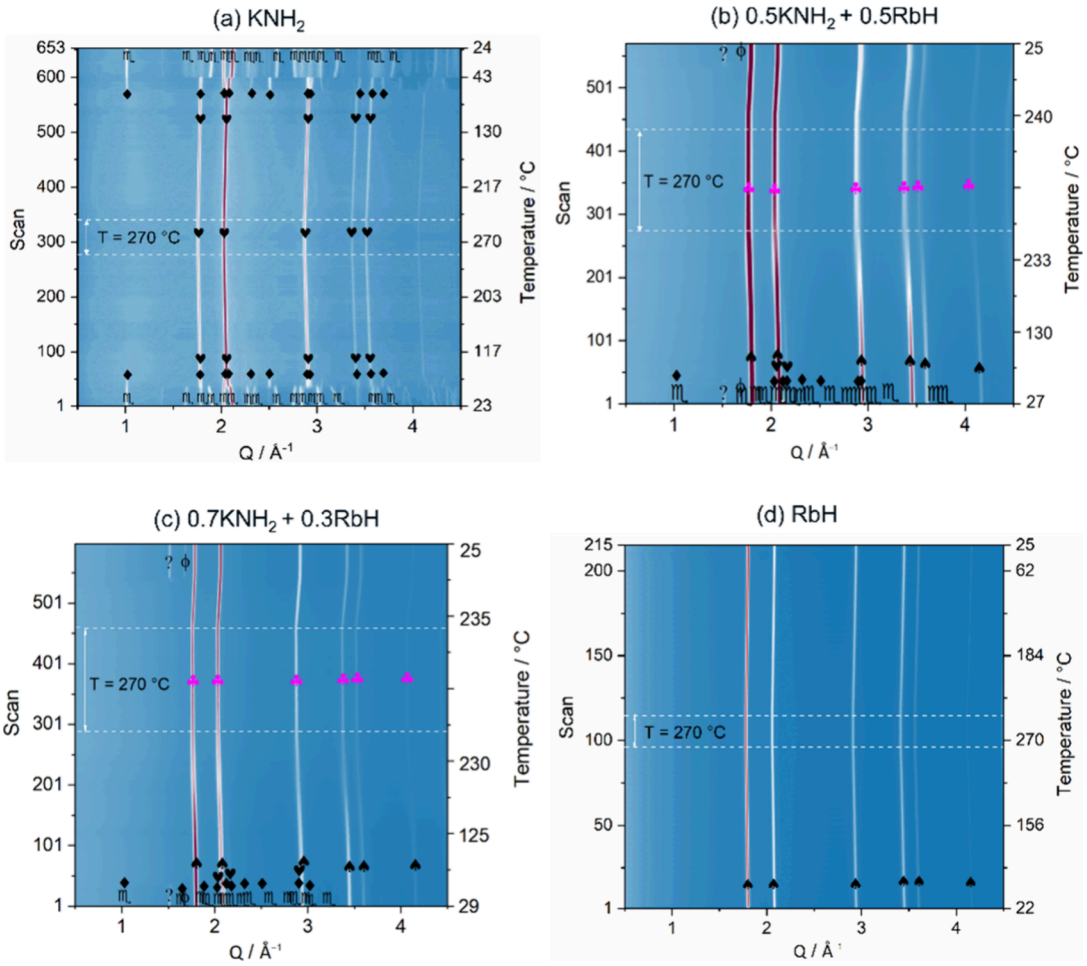

Figure 3. In situ SR-PXD data of the (a) KNH_2, (b) $0.5KNH_2 + 0.5RbH$, (c) $0.7KNH_2 + 0.3RbH$, and (d) RbH. ♣ = Rb−K−N−H solid solution ($Fm\bar{3}m$), ♏ = KNH_2 ($P2_1/m$), ♦ = KNH_2 ($P4/nmm$), ♥ = KNH_2 ($Fm\bar{3}m$), ♠ = RbH ($Fm\bar{3}m$), ϕ = K ($Im\bar{3}m$), and ? = unknown phase.

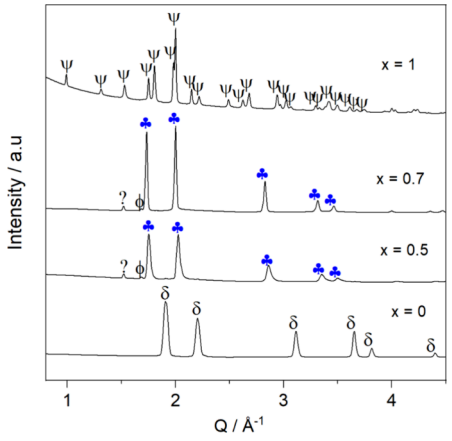

Figure 4. RT XRD data of the $x\mathrm{RbNH_2} + (1 - x)\mathrm{KH}$ samples after annealing at 270 °C, with $x = \{0, 0.5, 0.7, 1\}$. ψ = $RbNH_2$ ($P2_1/m$), δ = KH ($Fm\bar{3}m$), ♣ = Rb−K−N−H solid solution ($Fm\bar{3}m$), ϕ = K ($Im\bar{3}m$), and ? = unknown phase.

broadening is also observed for the $x = 0.5$ composition. This will be discussed in detail in the Rietveld refinements of XRD data, which are displayed in Figures 6 and 7.

As before, the phase evolution under real conditions was monitored with the conduction of in situ SR-PXD measurements. As shown in Figure 5, the in situ SR-PXD data of the $x\mathrm{RbNH_2} + (1 - x)\mathrm{KH}$ samples, where $x = \{0, 0.5, 0.7, 1\}$, were also collected. The in situ SR-PXD data of starting material $RbNH_2$ show a phase transition of $RbNH_2$ from a monoclinic (s.g. $P2_1/m$, labeled ψ) to a cubic structure (s.g. $Fm\bar{3}m$, labeled φ) at around 68 °C, while the RT-cubic structure of KH (s.g. $Fm\bar{3}m$, labeled δ) does not undergo a phase transition under the given experimental conditions, similar to the RbH. These results agree with those reported in refs 16 and 31. For compositions with $x = \{0.5, 0.7\}$, their in situ SR-PXD data show similarities, i.e., both show the transformation of $RbNH_2$ from the monoclinic (ψ) to the cubic (φ) structure at about 65 °C during heating, as expected. Subsequently, the mutual dissolution of $RbNH_2$ and KH takes place, accompanied by the substitution process of cubic $RbNH_2$ (φ) and cubic KH (δ) peaks observed starting from a temperature of about 150 °C and further increased during the isothermal period. As a result, the completion of solubility is achieved and the formation of a single cubic solid solution is observed for both compositions with $x = \{0.5, 0.7\}$, similar to the KNH_2−RbH system. In addition, metallic K (ϕ) and an unknown phase (?) are observed at room temperature, similarly to the KNH_2−RbH system.

To elucidate phase compositions in the mixed samples, Rietveld refinement of in situ SR-PXD data was performed (Rietveld refinement details can be found in ESI-Figure S4). Figure 6 and Table 1 present the Rietveld refinements of

https://doi.org/10.1021/acs.inorgchem.4c01016
Inorg. Chem. 2024, 63, 11233−11241

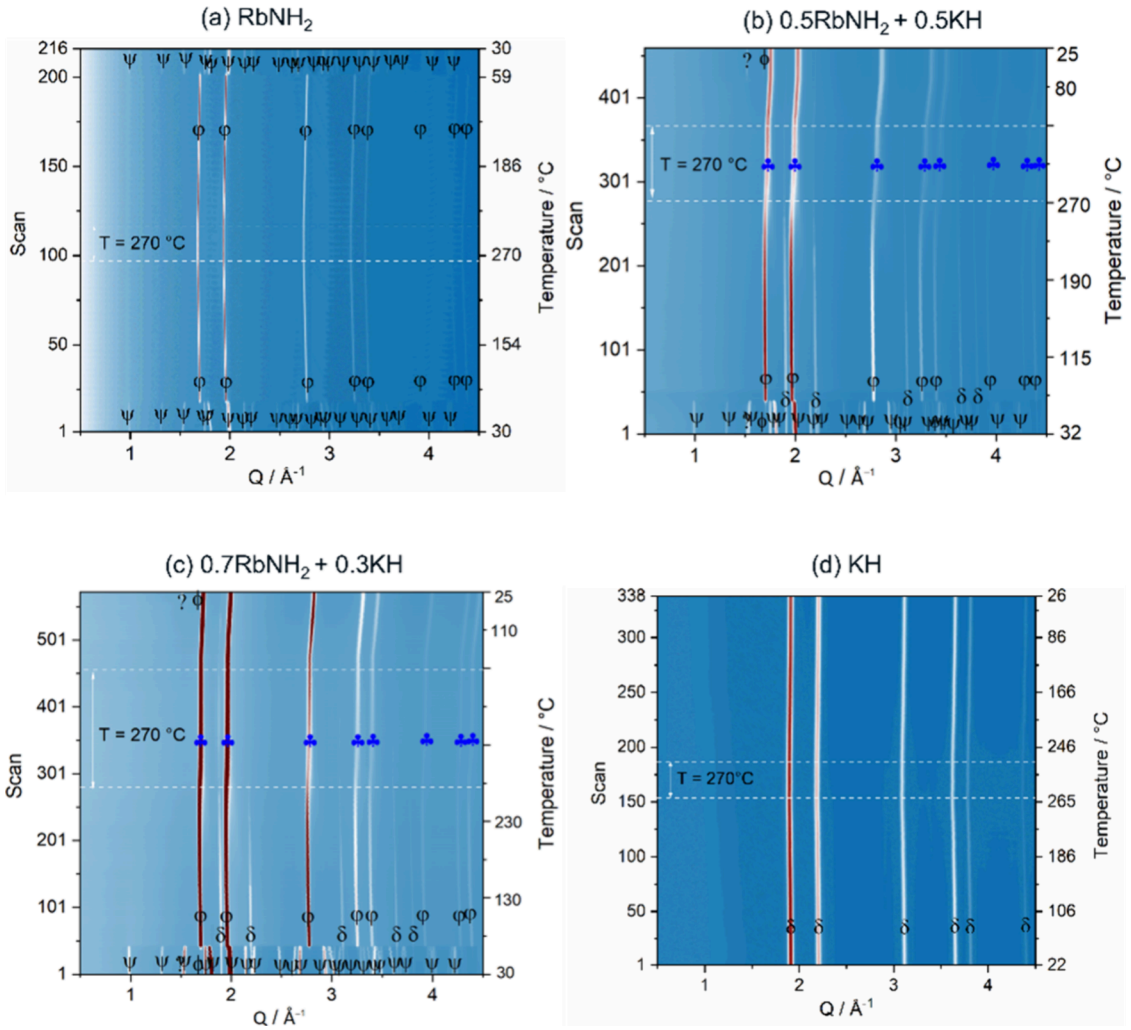

Figure 5. In situ SR-PXD data of the (a) $RbNH_2$, (b) $0.5RbNH_2 + 0.5KH$, (c) $0.7RbNH_2 + 0.3KH$, and (d) KH. ψ = $RbNH_2$ ($P2_1/m$), φ = $RbNH_2$ ($Fm\bar{3}m$), δ = KH ($Fm\bar{3}m$), ♣ = Rb−K−N−H solid solution ($Fm\bar{3}m$), ϕ = K ($Im\bar{3}m$), and ? = unknown phase.

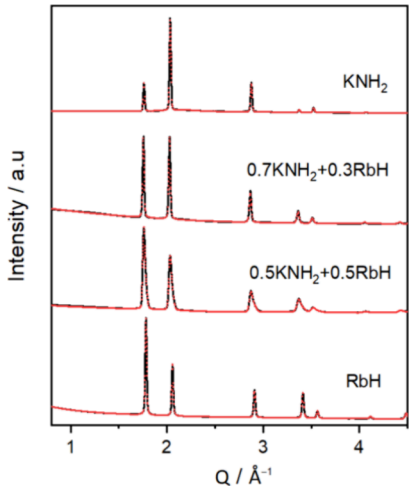

Figure 6. Rietveld refinements of the in situ SR-PXD data collected at 270 °C for $xKNH_2 + (1 - x)$RbH samples, where x = {0, 0.5, 0.7, 1}.

diffraction data collected at 270 °C and cell parameters of phases within the KNH_2−RbH system. For the x = {0.5, 0.7} compositions, the results confirmed the formation of a single cubic solid solution this these mixtures, also considering the partial desorption of ammonia and hydrogen during heating. Additionally, unreacted RbH is also observed for the x = 0.5 sample, indicating a not complete solubility of amide and hydride at this temperature. Similarly, for the $RbNH_2$−KH system, Rietveld refinement of XRD data is performed, as depicted in Figure 7 and Table 2. For the x = 0.7 sample, a single cubic solid solution of amide and hydride is formed, while for the x = 0.5 sample, an overlap of two solid solution phases corresponding to broader peaks observed in the XRD diffraction data is detected. Additionally, unreacted KH is also observed. Tables 1 and 2 present the phase compositions and lattice parameters of phases in both systems. The existence of cubic polymorphs of KNH_2 and $RbNH_2$ at temperature higher

Table 1. Lattice Parameters of the Solid Solution in the KNH_2−RbH System Obtained from the Rietveld Refinement of the SR-PXD Patterns Acquired at 270 °C

system 1	phase compositions	unit cell (a/Å)
KNH_2	KNH_2	6.19766
$0.7KNH_2 + 0.3RbH$	$Rb_{0.8}K_{0.2}(NH_2)_{0.4}H_{0.6}$ (100 wt %)	6.17582
$0.5KNH_2 + 0.5RbH$	$Rb_{0.9}K_{0.1}(NH_2)_{0.44}H_{0.56}$ (78.9 wt %)	6.17899
	RbH-like cubic (21.1 wt %)	6.10120
RbH	RbH	6.10687

https://doi.org/10.1021/acs.inorgchem.4c01016
Inorg. Chem. 2024, 63, 11233−11241

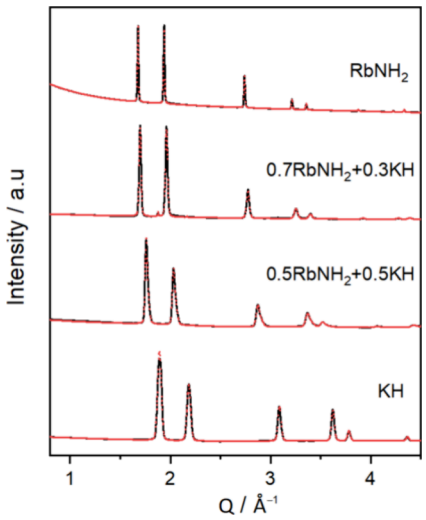

Figure 7. Rietveld refinements of the in situ SR-PXD data collected at 270 °C for xRbNH$_2$ + (1 − x)KH samples, where x = {0, 0.5, 0.7, 1}.

Table 2. Lattice Parameters of the Solid Solution in the RbNH$_2$−KH System Obtained from the Rietveld Refinement of the SR-PXD Patterns Acquired at 270 °C

system 2	phase compositions	unit cell (a/Å)
RbNH$_2$	RbNH$_2$	6.48491
0.7RbNH$_2$ + 0.3KH	$Rb_{0.77}K_{0.23}(NH_2)_{0.68}H_{0.32}$ (97.4 wt %)	6.38822
	KH-like cubic (2.6 wt %)	5.78233
0.5RbNH$_2$ + 0.5KH	$Rb_{0.94}K_{0.06}(NH_2)_{0.91}H_{0.09}$ (48.2 wt %)	6.32481
	$K_{0.99}(Rb_{0.01})NH_2$ (48 wt %)	6.23548
	KH-like cubic (3.8 wt %)	5.77403
KH	KH	5.74913

than 75 °C and their structural similarities with RbH and KH (e.g., cation and anion radii: r_{K+} = 1.52 Å, r_{Rb+} = 1.66 Å, r_{NH2-} = 1.73 Å, r_{H-} = 1.53 Å and cell parameters at 270 °C: KNH$_2$ (a = 6.19766 Å), RbNH$_2$ (a = 6.10687 Å), KH (a = 5.74913 Å), and RbH (a = 6.10687 Å)) pave the path to the formation of mixed solid solutions. It is observed that for the KNH$_2$−RbH system, the cubic KNH$_2$ likely dissolves into the cubic RbH structure, as seen by the disappearance of the KNH$_2$ diffraction peaks and the change in the RbH peaks (in situ XRD data in Figure 3). In contrast, the cubic KH dissolves into the cubic RbNH$_2$, detected by the shift of RbNH$_2$ peaks at $T \sim 270$ °C, when the solubility takes place (in situ XRD data in Figure 5). Besides, the diffraction data of the two systems (i.e., KNH$_2$−RbH (Figure 6) and RbNH$_2$−KH (Figure 7)) also show that the diffraction peaks are shifted, and their relative intensity varies gradually with increasing the amount of amide (i.e., x). This is indicative of the expected ionic substitution and change of the unit cell (see Tables 1 and 2).

The vibrational frequencies of the NH$_2$ group in the pure amides and mixed amide-hydride samples were characterized by FT-IR. As shown in ESI-Figure S5a for the KNH$_2$−RbH system, the stretching vibrational modes of the N−H bonds in KNH$_2$ are observed at 3253 and 3207 cm^{-1}. These signals slightly shift to lower frequencies in the mixed amide-hydride samples, probably due to volume expansion, which increases the N−H bond length, and the ionic substitution (K with Rb). In addition, the magnitude of these bands is weaker in the mixed samples with a reduced amount of amide compared to the original KNH$_2$, indicating the decrease of the dipole moment caused by the reduction of the negative charge on the nitrogen atom induced by a substituent such as hydrogen. This observation is similar to what has been observed in the Cs−N−H system[32] and for C−H bonds.[37,38] Likewise, a similar observation on the vibrational modes is also found for the RbNH$_2$−KH system, where the intensity of the signals of the stretching modes decreases because of the low amount of amide in the samples (ESI-Figure S5b).

It is noteworthy that although partial desorption of ammonia and hydrogen is observed, the formation of mixed metal amide-hydride solid solution is evident. Further confirmation of the solid solution formation for the KNH$_2$−RbH and RbNH$_2$−KH systems was achieved by solid-state NMR measurements. Figure 8a shows the ^{1}H MAS spectra of the 0.5KNH$_2$ + 0.5RbH and 0.5RbNH$_2$ + 0.5KH systems. In both spectra, similar chemical shifts for the hydride (6.2−6.3 ppm) and amide (−2.9 ppm) anions are observed, indicating the similarity of the chemical environment between these two mixed samples. Important note that, the presence of imide is not notied, thi

A direct assessment of the solid solution formation was provided by the 2D ^{1}H DQ MAS spectra, as shown in Figure 8b,c. For the 0.5KNH$_2$ + 0.5RbH sample (Figure 8b), the DQ correlation between the amide (δ_{SQ} = −2.9 ppm) and hydride (δ_{SQ} = 6.2 ppm) signals is observed at δ_{DQ} = 3.3 ppm. This implies that the protons of KNH$_2$ and RbH are in close spatial proximity to each other, i.e., within 3.5 Å, which implies that they belong to a homogeneous phase.[39,40] A similar correlation is also observed for the 0.5KNH$_2$ + 0.5RbH sample, where a DQ correlation between the amide (δ_{SQ} = −2.9 ppm) and the hydride (δ_{SQ} = 6.3 ppm) signals is found at δ_{DQ} = 3.4 ppm (Figure 8c), also indicating the intimate spatial proximity of the RbNH$_2$ and KH protons. The results of the in situ/ex situ XRD and SSNMR measurements provide adequate evidence to confirm the formation of solid solutions for both the KNH$_2$−RbH and RbNH$_2$−KH systems.

3.3. RbNH$_2$−CsH and CsNH$_2$−KH Systems. Extending the investigation in this line of research, we observed that solid solutions were also formed in the RbNH$_2$−CsH and CsNH$_2$−RbH systems. Figure 9 shows the phase evolution in these mixed amide-hydride composites in the temperature range from RT to 240 °C. As shown in Figure 9a for the in situ SR-PXD data of the RbNH$_2$−CsH composite, a phase transformation of RbNH$_2$ occurs, from a monoclinic (s.g. $P2_1/m$) to a cubic structure (s.g. $Fm\bar{3}m$), while the cubic CsH structure (s.g. $Fm\bar{3}m$) does not undergo any phase transition. These observations are similar to those reported earlier in this work and in ref 32. It is noted that at T > 65 °C, both RbNH$_2$ and CsH have similar crystal structures (s.g. $Fm\bar{3}m$), which might facilitate the ion mobility and consequently the formation of the solid solution. At the temperature of 240 °C, the disappearance of the cubic RbNH$_2$ phase and the change of the cubic CsH peaks are observed, indicating the mutual solubility of the RbNH$_2$ and CsH to form a solid solution with the same space group. This single cubic solid solution is stable and remains unchanged during cooling. Similarly, for the CsNH$_2$−RbH composite, the in situ SR-PXD data seen in Figure 9b show the phase transition of CsNH$_2$ from a tetragonal structure (s.g. $P4/nmm$) to cubic ones (s.g. $Pm\bar{3}m$ and $Fm\bar{3}m$), comparable to what was reported in ref 32, while the cubic RbH structure (s.g. $Fm\bar{3}m$) remains stable. A single

https://doi.org/10.1021/acs.inorgchem.4c01016
Inorg. Chem. 2024, 63, 11233−11241

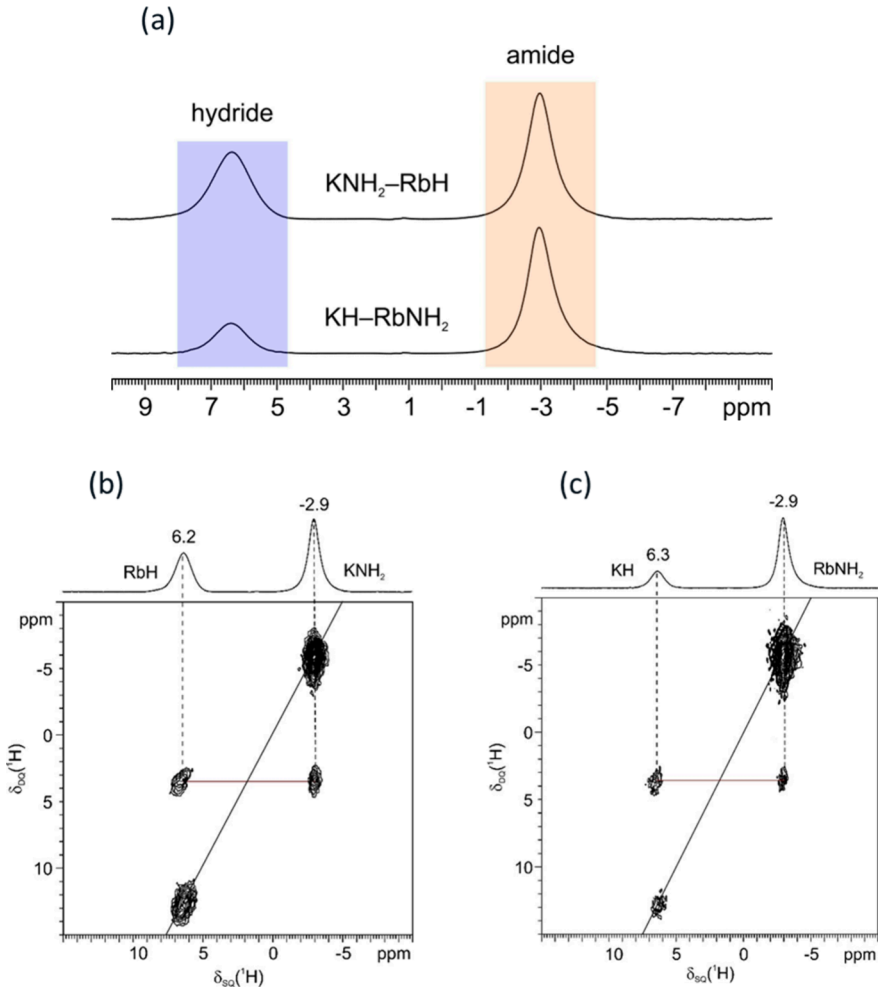

Figure 8. (a) ^{1}H (600.13 MHz) MAS SSNMR spectra of the 0.5KNH_2 + 0.5RbH and 0.5$RbNH_2$ + 0.5KH compositions, acquired at probe temperature at a spinning speed of 20 kHz; 2D ^{1}H (600.13 MHz) DQ MAS SSNMR spectra of the (b) 0.5KNH_2 + 0.5RbH and (c) 0.5$RbNH_2$ + 0.5KH systems, recorded at a spinning speed of 20 kHz at probe temperature. Red lines highlight the DQ correlation between the amide and hydride signals in both systems.

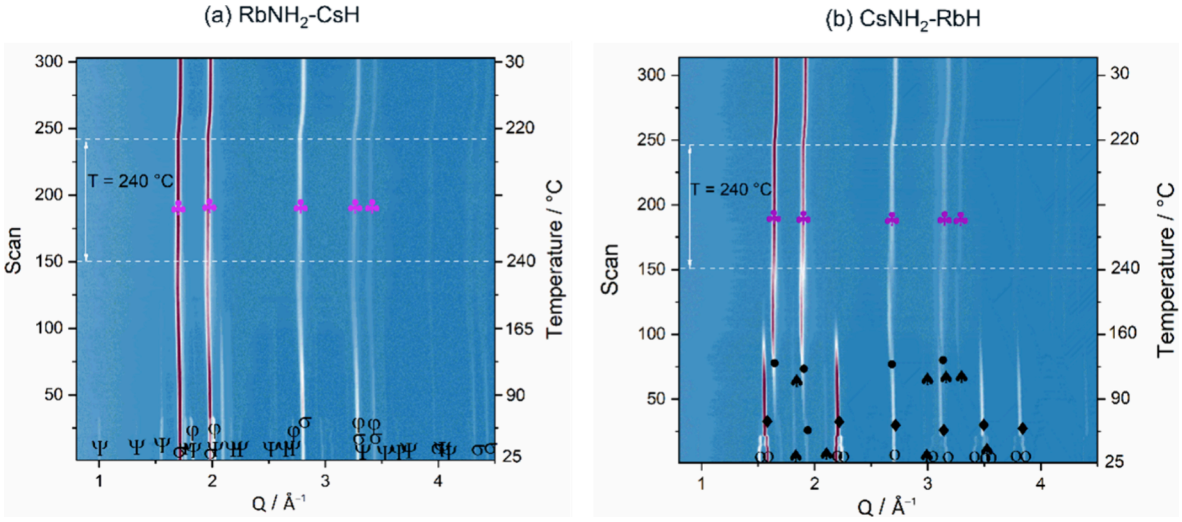

Figure 9. In situ SR-PXD data of the $RbNH_2$−CsH (a) and $CsNH_2$−RbH (b) composites. Ψ = $RbNH_2$ ($P2_1/m$), φ = $RbNH_2$ ($Fm\bar{3}m$), σ = CsH ($Fm\bar{3}m$), ♣ = $RbNH_2$−CsH solid solution ($Fm\bar{3}m$). o = $CsNH_2$ ($P4/nmm$), ♦ = $CsNH_2$ ($Pm\bar{3}m$), • = $CsNH_2$ ($Fm\bar{3}m$), ♠ = RbH ($Fm\bar{3}m$), and ♣ = $CsNH_2$−RbH solid solution ($Fm\bar{3}m$).

cubic phase (s.g. $Fm\bar{3}m$) is observed at the isothermal temperature of 240 °C, indicating the mutual solubility of RbH and $CsNH_2$. This $CsNH_2$−RbH cubic solid solution is stable during cooling. The results derived from the in situ SR-

https://doi.org/10.1021/acs.inorgchem.4c01016
Inorg. Chem. 2024, 63, 11233−11241

PXD data of $RbNH_2$−CsH and $CsNH_2$−RbH are comparable to those obtained for the KNH_2−RbH and $RbNH_2$−KH systems. Therefore, it is reasonable to assume that the formation of a solid solution was similarly achieved for these systems.

4. CONCLUSIONS

In this work, the formation of solid solutions in the amide-hydride system of alkali metals (K, Rb, and Cs), namely, KNH_2−RbH, $RbNH_2$−KH, $RbNH_2$−CsH, and $CsNH_2$−RbH, has been elucidated by various techniques (i.e., ^{1}H 1D and 2D SSNMR, FT-IR, and ex situ/in situ XRD), leading to the following conclusive points:

Due to the structural and physicochemical similarities between MNH_2 amide and MH hydride, the mixed metal solid solutions are formed by both cation and anion exchange.

The formed MNH_2-MH solid solutions such as $RbNH_2$−KH, KNH_2−RbH, $RbNH_2$−CsH, etc., could replace ionic hydrides (KH, RbH, and CsH) as additives for hydrogen storage systems. Follow-up research will be conducted to investigate the hydrogen storage properties of the $Mg(NH_2)_2$-2LiH system in the presence of mixed alkali amide-hydride solid solutions.

It is worth noting that the formation of mixed metal amide-hydride solid solutions with an expanded lattice could lead to disorder of the crystal structure (due to the size difference between cations and anions substituted) and possibly facilitate the ion transport. This aspect will be further investigated in a future work.

The findings of this work, in conjunction with our earlier studies on the amide-hydride solid solutions, serve as the foundation for additional research aimed at expanding this area of study and identifying analogies with other systems.

■ ASSOCIATED CONTENT

Supporting Information

The Supporting Information is available free of charge at https://pubs.acs.org/doi/10.1021/acs.inorgchem.4c01016.

MS data, Rietveld refinement data, and FT-IR spectra (PDF)

■ AUTHOR INFORMATION

Corresponding Authors

Thi Thu Le − *Institute of Hydrogen Technology, Helmholtz-Zentrum hereon GmbH, Geesthacht D-21502, Germany*; Email: thi.le@hereon.de

Claudio Pistidda − *Institute of Hydrogen Technology, Helmholtz-Zentrum hereon GmbH, Geesthacht D-21502, Germany*; orcid.org/0000-0002-0706-6972; Email: claudio.pistidda@hereon.de

Authors

Simone Bordignon − *Department of Chemistry, University of Torino, Torino I-10125, Italy*

Michele R. Chierotti − *Department of Chemistry, University of Torino, Torino I-10125, Italy*; orcid.org/0000-0002-8734-6009

Yuanyuan Shang − *Institute of Hydrogen Technology, Helmholtz-Zentrum hereon GmbH, Geesthacht D-21502, Germany*

Alexander Schökel − *Deutsches Elektronen-Synchrotron DESY, Hamburg D-22607, Germany*; orcid.org/0000-0002-3680-8648

Thomas Klassen − *Institute of Hydrogen Technology, Helmholtz-Zentrum hereon GmbH, Geesthacht D-21502, Germany; Helmut Schmidt University, Hamburg D-22043, Germany*

Complete contact information is available at: https://pubs.acs.org/10.1021/acs.inorgchem.4c01016

Author Contributions

T.-T.L.: conceptualization, methodology, formal analysis, investigation, validation, and writing-original draft preparation; S.B. and M.R.C.: resources and investigation; Y.S.: investigation; A.S.: resources; T.K.: supervision and funding acquisition; C.P.: supervision; and all authors contributed to revising the manuscript.

Notes

The authors declare no competing financial interest.

■ ACKNOWLEDGMENTS

This research is funded by dtec. bw—Digitalization and Technology Research Center of Bundeswehr which we gratefully acknowledge.

■ REFERENCES

(1) Chen, P.; Xiong, Z.; Luo, J.; Lin, J.; Tan, K. L. Interaction of hydrogen with metal nitrides and imides. *Nature* **2002**, *420* (6913), 302−304.

(2) Ichikawa, T.; Isobe, S.; Hanada, N.; Fujii, H. Lithium nitride for reversible hydrogen storage. *J. Alloys Compd.* **2004**, *365* (1), 271−276.

(3) Chen, P.; Xiong, Z.; Luo, J.; Lin, J.; Tan, K. L. Interaction between Lithium Amide and Lithium Hydride. *J. Phys. Chem. B* **2003**, *107* (39), 10967−10970.

(4) Xiong, Z.; Wu, G.; Hu, J.; Chen, P. Ternary Imides for Hydrogen Storage. *Adv. Mater.* **2004**, *16* (17), 1522−1525.

(5) Hino, S.; Ichikawa, T.; Ogita, N.; Udagawa, M.; Fujii, H. Quantitative estimation of NH3 partial pressure in H2 desorbed from the Li−N−H system by Raman spectroscopy. *Chem. Commun.* **2005**, *24*, 3038−3040.

(6) Makepeace, J. W.; Brittain, J. M.; Sukhwani Manghnani, A.; Murray, C. A.; Wood, T. J.; David, W. I. F. Compositional flexibility in Li−N−H materials: implications for ammonia catalysis and hydrogen storage. *Phys. Chem. Chem. Phys.* **2021**, *23* (28), 15091−15100.

(7) Ichikawa, T.; Tokoyoda, K.; Leng, H.; Fujii, H. Hydrogen absorption properties of Li−Mg−N−H system. *J. Alloys Compd.* **2005**, *400* (1), 245−248.

(8) Orimo, S.; Nakamori, Y.; Kitahara, G.; Miwa, K.; Ohba, N.; Noritake, T.; Towata, S. Destabilization and enhanced dehydriding reaction of LiNH2: an electronic structure viewpoint. *Appl. Phys. A: Mater. Sci. Process.* **2004**, *79* (7), 1765−1767.

(9) Luo, W.; Rönnebro, E. Towards a viable hydrogen storage system for transportation application. *J. Alloys Compd.* **2005**, *404*−*406*, 392−395.

(10) Luo, W.; Sickafoose, S. Thermodynamic and structural characterization of the Mg−Li−N−H hydrogen storage system. *J. Alloys Compd.* **2006**, *407* (1), 274−281.

(11) Xiong, Z.; Hu, J.; Wu, G.; Chen, P.; Luo, W.; Gross, K.; Wang, J. Thermodynamic and kinetic investigations of the hydrogen storage in the Li−Mg−N−H system. *J. Alloys Compd.* **2005**, *398* (1), 235−239.

(12) Aslan, N.; Gizer, G.; Pistidda, C.; Dornheim, M.; Müller, M.; Busch, S.; Lohstroh, W. High Hydrogen Mobility in an Amide−Borohydride Compound Studied by Quasielastic Neutron Scattering. *Adv. Eng. Mater.* **2021**, *23* (11), No. 2100620.

(13) Gizer, G.; Puszkiel, J.; Cao, H.; Pistidda, C.; Le, T. T.; Dornheim, M.; Klassen, T. Tuning the reaction mechanism and hydrogenation/dehydrogenation properties of 6Mg(NH2)29LiH system by adding LiBH4. *Int. J. Hydrogen Energy* **2019**, *44* (23), 11920−11929.
(14) Gizer, G.; Puszkiel, J.; Riglos, M. V. C.; Pistidda, C.; Ramallo-López, J. M.; Mizrahi, M.; Santoru, A.; Gemming, T.; Tseng, J.-C.; Klassen, T.; Dornheim, M. Improved kinetic behaviour of Mg(NH2)-2−2LiH doped with nanostructured K-modified-LixTiyOz for hydrogen storage. *Sci. Rep.* **2020**, *10* (1), 8.
(15) Santoru, A.; Garroni, S.; Pistidda, C.; Milanese, C.; Girella, A.; Marini, A.; Masolo, E.; Valentoni, A.; Bergemann, N.; Le, T. T.; Cao, H.; Haase, D.; Balmes, O.; Taube, K.; Mulas, G.; Enzo, S.; Klassen, T.; Dornheim, M. A new potassium-based intermediate and its role in the desorption properties of the K−Mg−N−H system. *Phys. Chem. Chem. Phys.* **2016**, *18* (5), 3910−3920.
(16) Santoru, A.; Pistidda, C.; Brighi, M.; Chierotti, M. R.; Heere, M.; Karimi, F.; Cao, H.; Capurso, G.; Chaudhary, A.-L.; Gizer, G.; Garroni, S.; Sørby, M. H.; Hauback, B. C.; Černý, R.; Klassen, T.; Dornheim, M. Insights into the Rb−Mg−N−H System: an Ordered Mixed Amide/Imide Phase and a Disordered Amide/Hydride Solid Solution. *Inorg. Chem.* **2018**, *57* (6), 3197−3205.
(17) Boukamp, B. A.; Huggins, R. A. Ionic conductivity in lithium imide. *Phys. Lett. A* **1979**, *72* (6), 464−466.
(18) Wang, J.; Lei, G.; He, T.; Cao, H.; Chen, P. Defect-rich potassium amide: A new solid-state potassium ion electrolyte. *Journal of Energy Chemistry* **2022**, *69*, 555−560.
(19) Matsuo, M.; Remhof, A.; Martelli, P.; Caputo, R.; Ernst, M.; Miura, Y.; Sato, T.; Oguchi, H.; Maekawa, H.; Takamura, H.; Borgschulte, A.; Züttel, A.; Orimo, S.-I Complex Hydrides with (BH4)−and (NH2)−Anions as New Lithium Fast-Ion Conductors. *J. Am. Chem. Soc.* **2009**, *131* (45), 16389−16391.
(20) Cao, H.; Zhang, Y.; Wang, J.; Xiong, Z.; Wu, G.; Chen, P. Materials design and modification on amide-based composites for hydrogen storage. *Progress in Natural Science: Materials International* **2012**, *22* (6), 550−560.
(21) Santoru, A.; Garroni, S.; Pistidda, C.; Milanese, C.; Girella, A.; Marini, A.; Masolo, E.; Valentoni, A.; Bergemann, N.; Le, T. T.; Cao, H.; Haase, D.; Balmes, O.; Taube, K.; Mulas, G.; Enzo, S.; Klassen, T.; Dornheim, M. A new potassium-based intermediate and its role in the desorption properties of the K-Mg-N-H system. *Phys. Chem. Chem. Phys.* **2016**, *18* (5), 3910−3920.
(22) Wang, J.; Chen, P.; Pan, H.; Xiong, Z.; Gao, M.; Wu, G.; Liang, C.; Li, C.; Li, B.; Wang, J. Solid−Solid Heterogeneous Catalysis: The Role of Potassium in Promoting the Dehydrogenation of the Mg(NH2)2/2 LiH Composite. *ChemSusChem* **2013**, *6* (11), 2181−2189.
(23) Durojaiye, T.; Hayes, J.; Goudy, A. Potassium, rubidium and cesium hydrides as dehydrogenation catalysts for the lithium amide/magnesium hydride system. *Int. J. Hydrogen Energy* **2015**, *40* (5), 2266−2273.
(24) Zhang, J.; Liu, Y.; Zhang, X.; Yang, Y.; Zhang, Q.; Jin, T.; Wang, Y.; Gao, M.; Sun, L.; Pan, H. Synthesis of CsH and its effect on the hydrogen storage properties of the Mg(NH2)2−2LiH system. *Int. J. Hydrogen Energy* **2016**, *41* (26), 11264−11274.
(25) Zhang, J.; Wang, Y.; Zhang, M.; Leng, Z.; Gao, M.; Hu, J.; Liu, Y.; Pan, H. Improved overall hydrogen storage properties of a CsH and KH co-doped Mg(NH2)2/2LiH system by forming mixed amides of Li−K and Cs−Mg. *RSC Adv.* **2017**, *7* (48), 30357−30364.
(26) Kitano, M.; Inoue, Y.; Ishikawa, H.; Yamagata, K.; Nakao, T.; Tada, T.; Matsuishi, S.; Yokoyama, T.; Hara, M.; Hosono, H. Essential role of hydride ion in ruthenium-based ammonia synthesis catalysts. *Chemical Science* **2016**, *7* (7), 4036−4043.
(27) Le, T.-T.; Abbas, M.; Dreistadt, D. M.; Klassen, T.; Pistidda, C. Ionic conductivity in complex hydrides for energy storage applications: A comprehensive review. *Chemical Engineering Journal* **2023**, *473*, No. 145315.
(28) Maekawa, H.; Matsuo, M.; Takamura, H.; Ando, M.; Noda, Y.; Karahashi, T.; Orimo, S.-I. Halide-Stabilized LiBH4, a Room-Temperature Lithium Fast-Ion Conductor. *J. Am. Chem. Soc.* **2009**, *131* (3), 894−895.
(29) Matsuo, M.; Takamura, H.; Maekawa, H.; Li, H.-W.; Orimo, S.-I. Stabilization of lithium superionic conduction phase and enhancement of conductivity of LiBH4 by LiCl addition. *Appl. Phys. Lett.* **2009**, *94* (8), No. 084103.
(30) Matsuo, M.; Kuromoto, S.; Sato, T.; Oguchi, H.; Takamura, H.; Orimo, S.-I. Sodium ionic conduction in complex hydrides with [BH4]−and [NH2]−anions. *Appl. Phys. Lett.* **2012**, *100* (20), No. 203904.
(31) Santoru, A.; Pistidda, C.; Sørby, M. H.; Chierotti, M. R.; Garroni, S.; Pinatel, E.; Karimi, F.; Cao, H.; Bergemann, N.; Le, T. T.; Puszkiel, J.; Gobetto, R.; Baricco, M.; Hauback, B. C.; Klassen, T.; Dornheim, M. KNH2−KH: a metal amide−hydride solid solution. *Chem. Commun.* **2016**, *52* (79), 11760−11763.
(32) Le, T.-T.; Santhosh, A.; Bordignon, S.; Chierotti, M. R.; Jerabek, P.; Klassen, T.; Pistidda, C. Experimental and computational studies on the formation of mixed amide-hydride solid solutions for CsNH2−CsH system. *Results in Engineering* **2023**, *17*, No. 100895.
(33) Martins, R. V.; Schell, N.; Lippmann, T.; Beckmann, F.; Ruhnau, H.-U.; Kiehn, R.; Schreyer, A. The status of GKSS' high energy materials science beamline at Petra III. *Acta Crystallogr., Sect. A* **2007**, *63* (a1), No. s246. doi:
(34) Bösenberg, U.; Pistidda, C.; Tolkiehn, M.; Busch, N.; Saldan, I.; Suarez-Alcantara, K.; Arendarska, A.; Klassen, T.; Dornheim, M. Characterization of metal hydrides by in-situ XRD. *Int. J. Hydrogen Energy* **2014**, *39* (18), 9899−9903.
(35) Pistidda, C.; Santoru, A.; Garroni, S.; Bergemann, N.; Rzeszutek, A.; Horstmann, C.; Thomas, D.; Klassen, T.; Dornheim, M. First Direct Study of the Ammonolysis Reaction in the Most Common Alkaline and Alkaline Earth Metal Hydrides by in Situ SR-PXD. *J. Phys. Chem. C* **2015**, *119* (2), 934−943.
(36) Lutterotti, L.; Matthies, S.; Wenk, H. R.; Schultz, A. S.; Richardson, J. W. Combined texture and structure analysis of deformed limestone from time-of-flight neutron diffraction spectra. *J. Appl. Phys.* **1997**, *81* (2), 594−600.
(37) Cinar, M.; Coruh, A.; Karabacak, M. FT-IR, UV−vis, 1H and 13C NMR spectra and the equilibrium structure of organic dye molecule disperse red 1 acrylate: A combined experimental and theoretical analysis. *Spectrochimica Acta Part A: Molecular and Biomolecular Spectroscopy* **2011**, *83* (1), 561−569.
(38) Spedding, H.; Whiffen, D. H. Intensities in the Infra-Red Spectrum of Benzene. *Proc. R. Soc. London, Ser. A: Math. Phys. Sci.* **1956**, *238* (1213), 245−255.
(39) Griffin, J. M.; Martin, D. R.; Brown, S. P. Distinguishing Anhydrous and Hydrous Forms of an Active Pharmaceutical Ingredient in a Tablet Formulation Using Solid-State NMR Spectroscopy. *Angew. Chem., Int. Ed.* **2007**, *46* (42), 8036−8038.
(40) Schnell, I.; Spiess, H. W. High-Resolution 1H NMR Spectroscopy in the Solid State: Very Fast Sample Rotation and Multiple-Quantum Coherences. *J. Magn. Reson.* **2001**, *151* (2), 153−227.

https://doi.org/10.1021/acs.inorgchem.4c01016
Inorg. Chem. 2024, 63, 11233−11241

Supporting Information

Mixed Metal Amide-Hydride Solid Solutions for Potential Energy Storage Applications

Thi Thu Le[a,], Simone Bordignon[b], Michele R. Chierotti[b], Yuanyuan Shang[a], Alexander Schökel[c], Thomas Klassen[a,d], Claudio Pistidda[a,*]*

[a]Institute of Hydrogen Technology, Helmholtz-Zentrum hereon GmbH, Max-Planck-Straße 1, D-21502 Geesthacht, Germany.

[b]Department of Chemistry - University of Torino, V. P. Giuria 7, I-10125, Torino, Italy.

[c]Deutsches Elektronen-Synchrotron DESY, Notkestraße 85, D-22607 Hamburg, Germany.

[d]Helmut Schmidt University, Holstenhofweg 85, D-22043 Hamburg, Germany.

*Corresponding authors: Thi Thu Le (thi.le@hereon.de); Claudio Pistidda (claudio.pistidda@hereon.de)

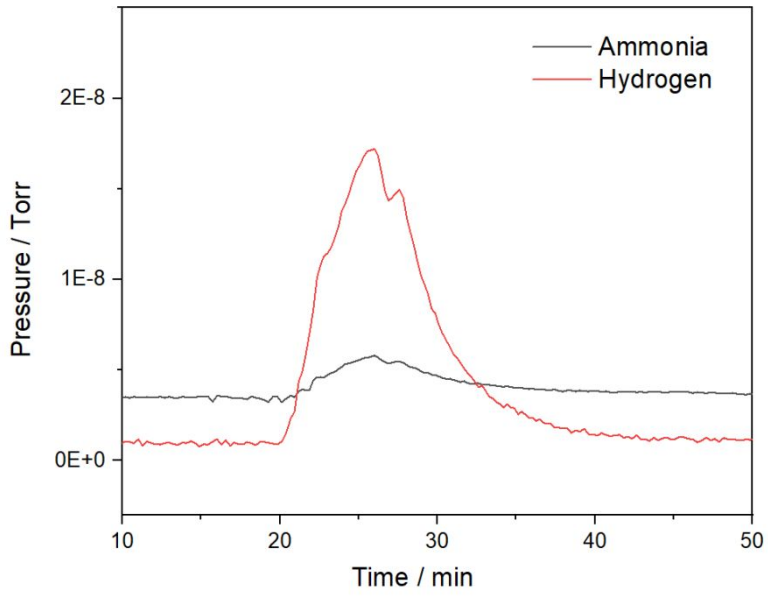

Figure S1. Gas evolution detected by mass spectrometer for the $0.7KNH_2$+0.3RbH during mixing.

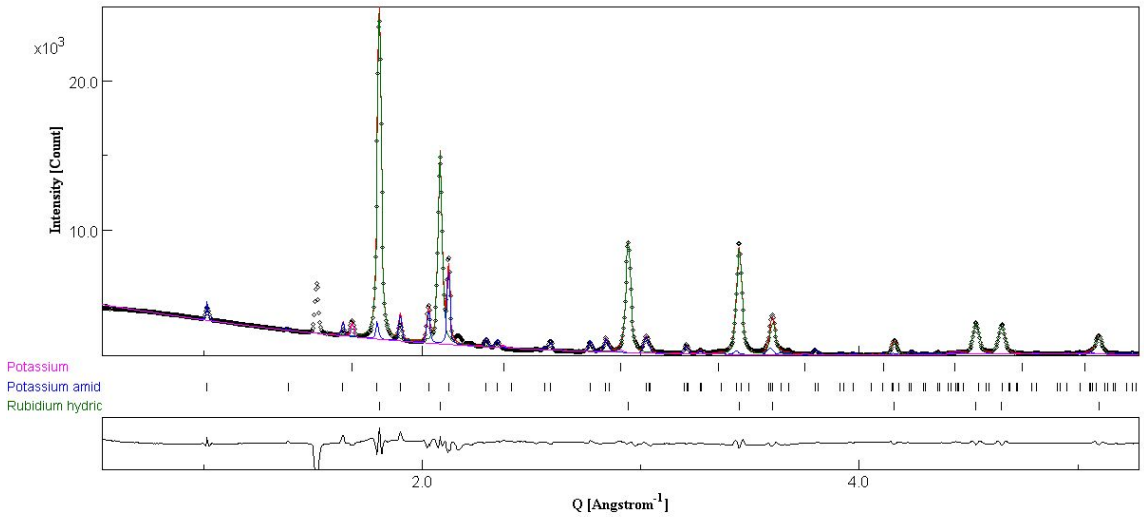

Figure S2. Rietveld refinement of the room temperature *in-situ* SP-PXD of $0.7KNH_2$+0.3RbH sample. Cell parameter of the RbH-like phase, a = 6.0405617 Å. R_{wp} = 5.8 %.

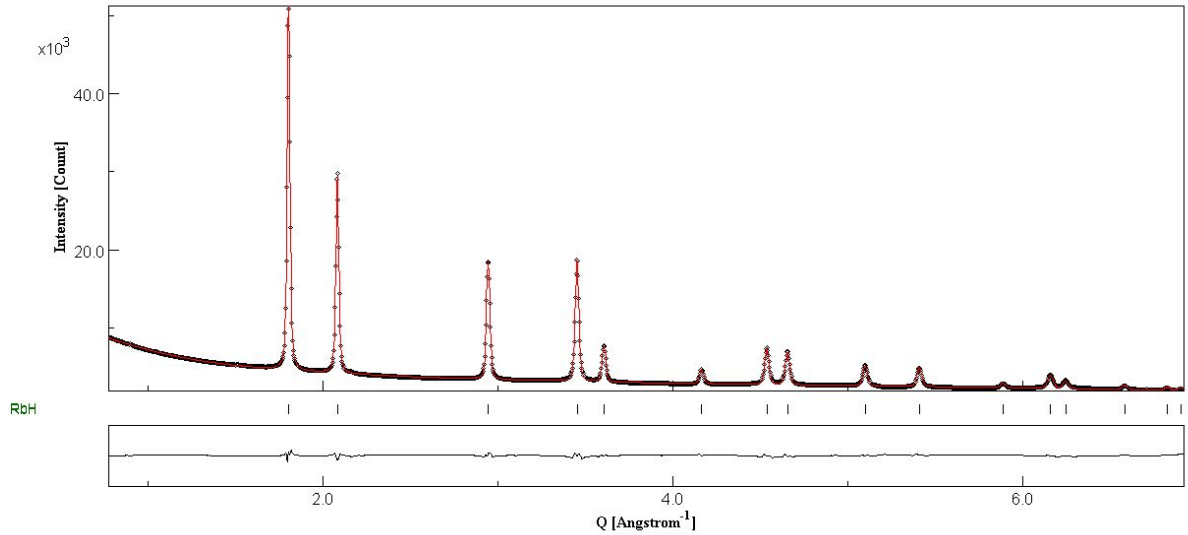

Figure S3. Rietveld refinement of the room temperature *in-situ* SP-PXD of the RbH sample. Cell parameter of the RbH: a = 6.0363336 Å. R_{wp} = 2.1 %.

(a) $RbNH_2$ (sigma = 0.80, R_{wp} = 1.33 %, R_{exp} = 1.66 %)

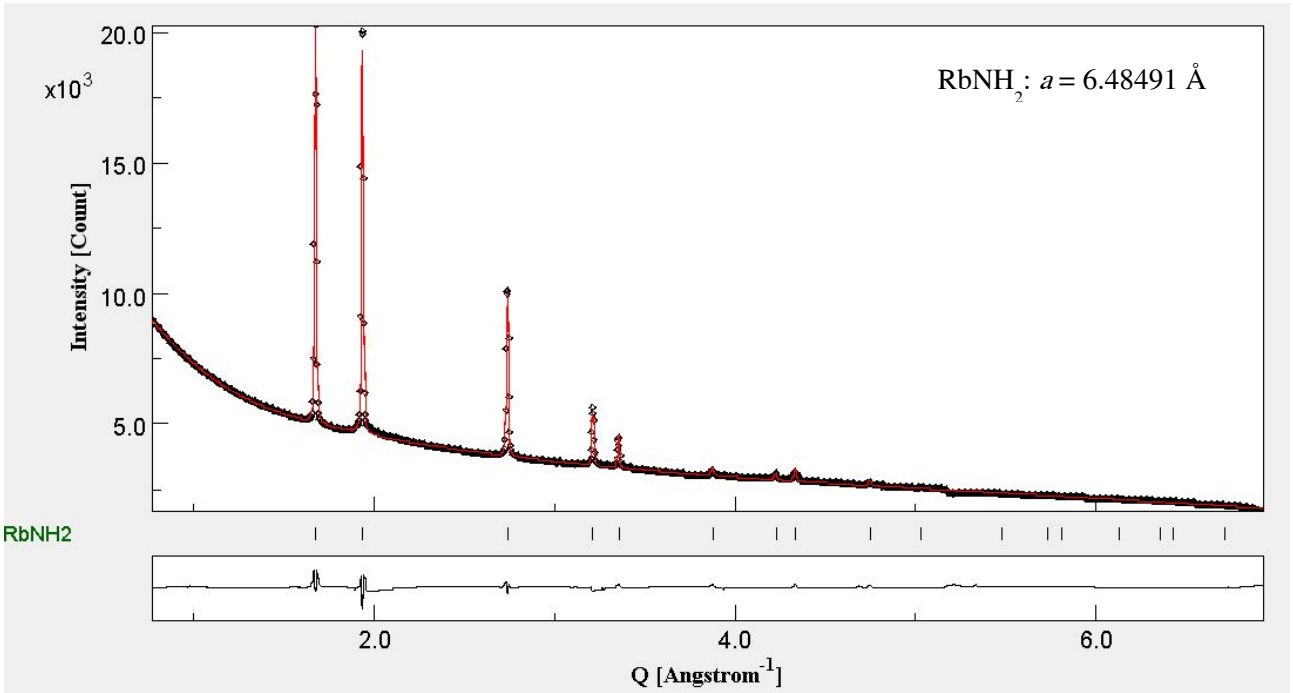

(b) KH (sigma = 2.18, R_{wp} = 4.14 %, R_{exp} = 1.90 %)

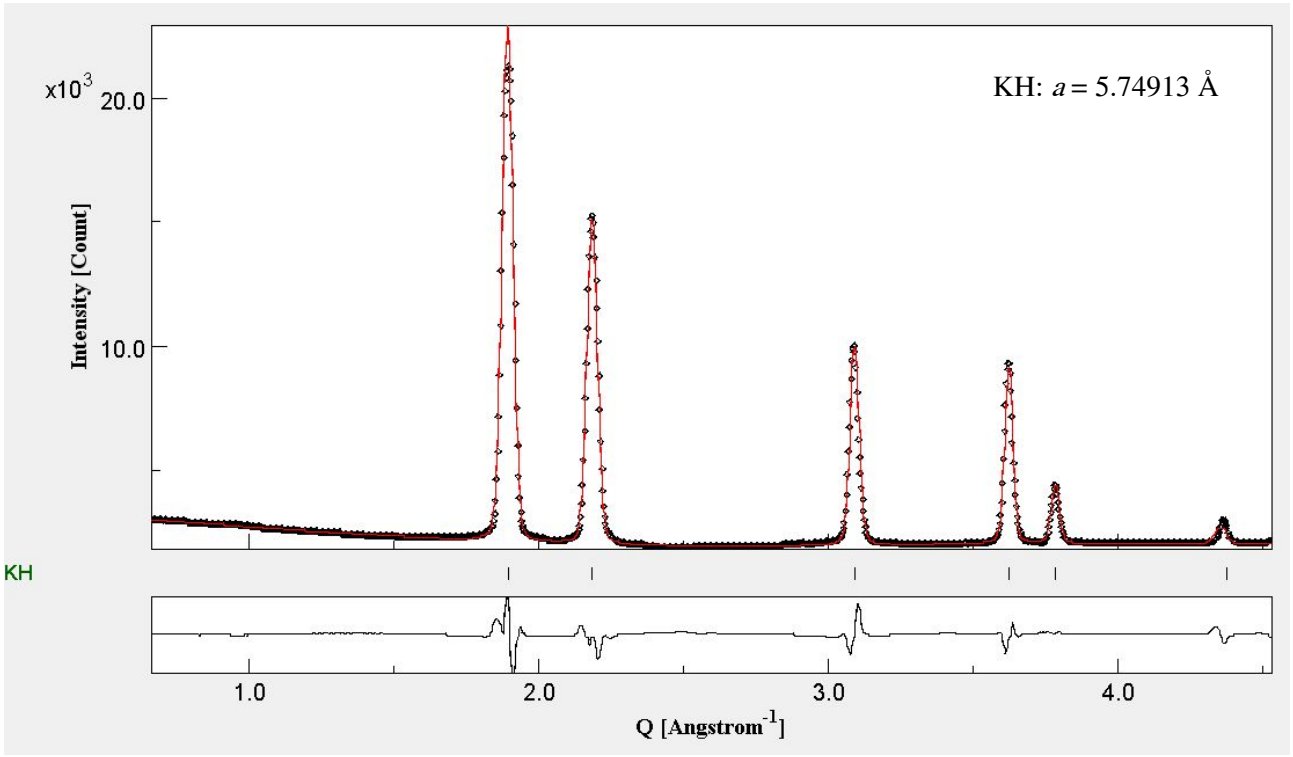

(c) 0.7$RbNH_2$+0.3KH (sigma = 2.0, R_{wp} = 3.24 %, R_{exp} = 1.62 %)

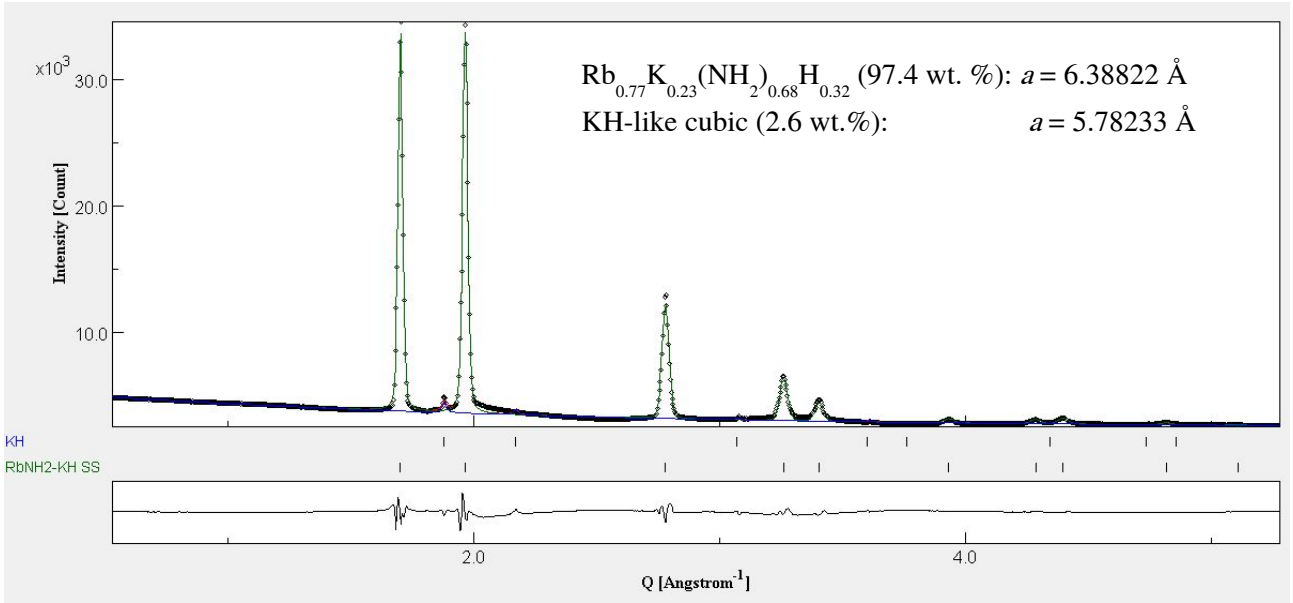

(d) 0.5$RbNH_2$+0.5KH (sigma = 1.30, R_{wp} = 2.30 %, R_{exp} = 1.77 %)

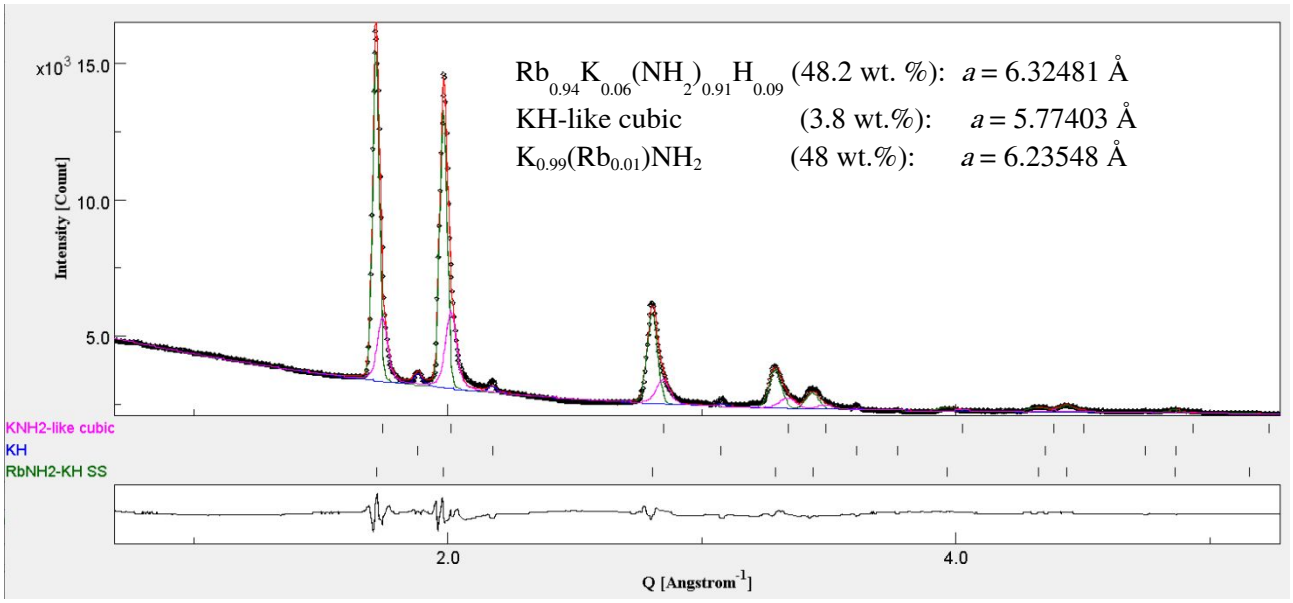

(e) KNH_2 (sigma = 0.51, R_{wp} = 3.58 %, R_{exp} = 7.07 %)

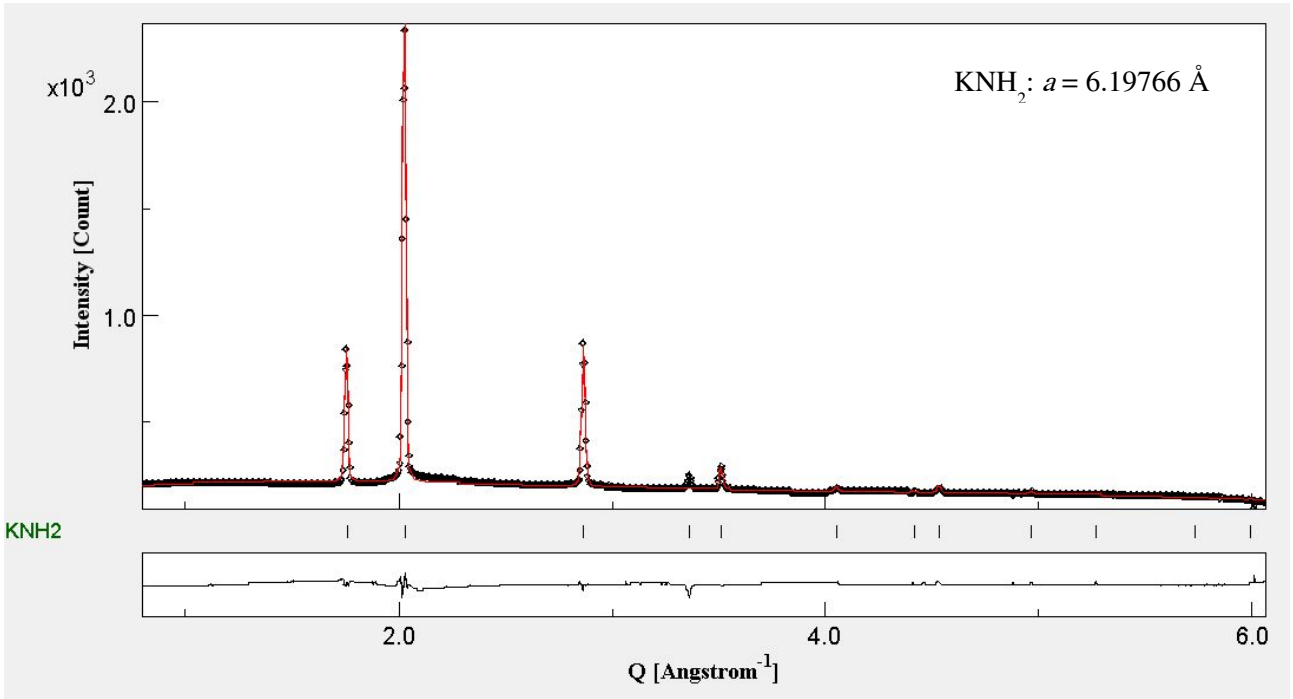

(f) RbH (sigma = 1.25, R_{wp} = 1.98 %, R_{exp} = 1.57 %)

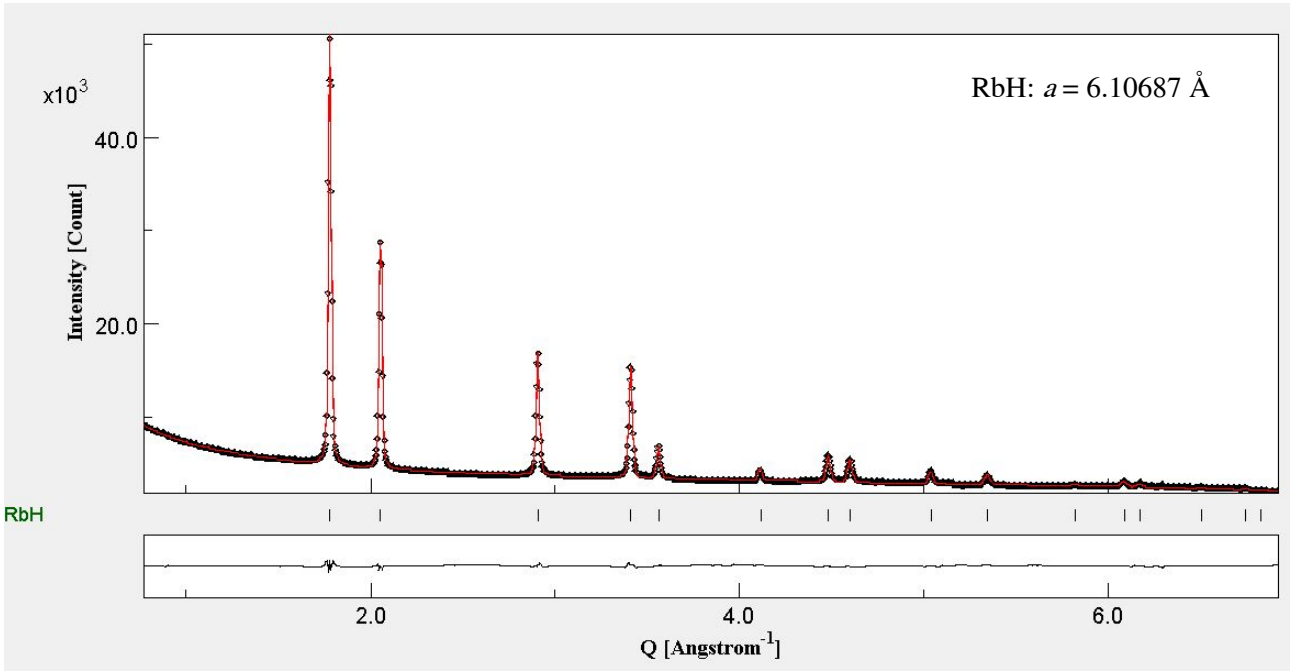

(g) 0.7KNH_2+0.3RbH (sigma = 1.41, R_{wp} = 2.62 %, R_{exp} = 1.84 %)

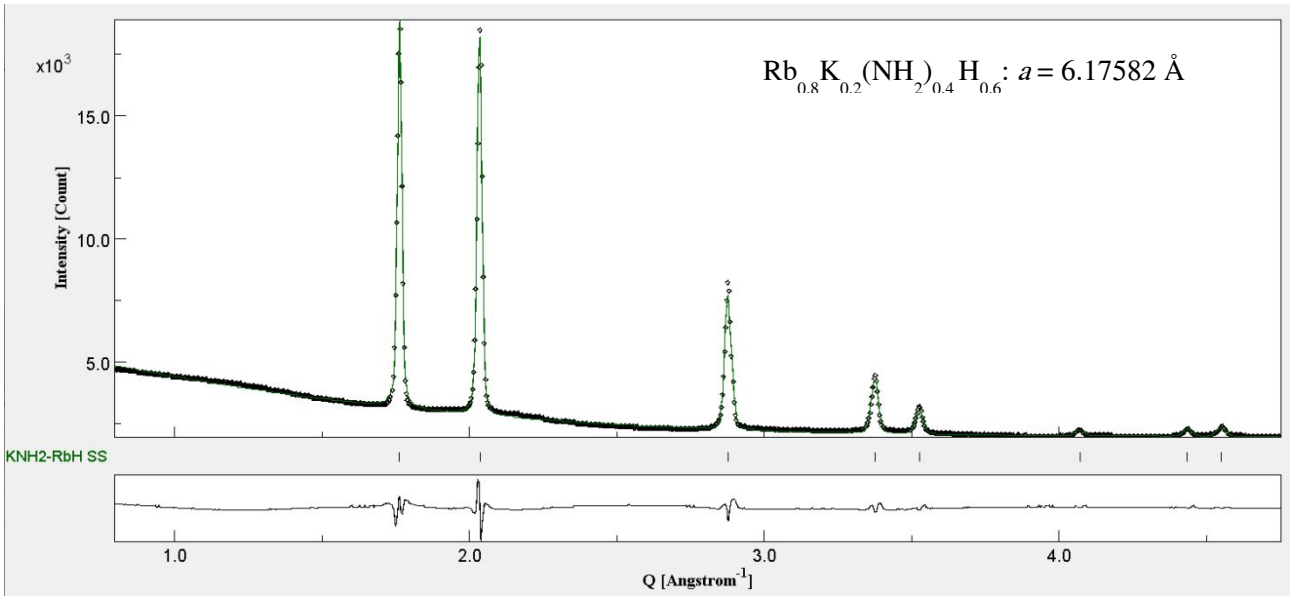

(h) 0.5KNH_2+0.5RbH (sigma = 2.24, R_{wp} = 3.86 %, R_{exp} = 1.72 %)

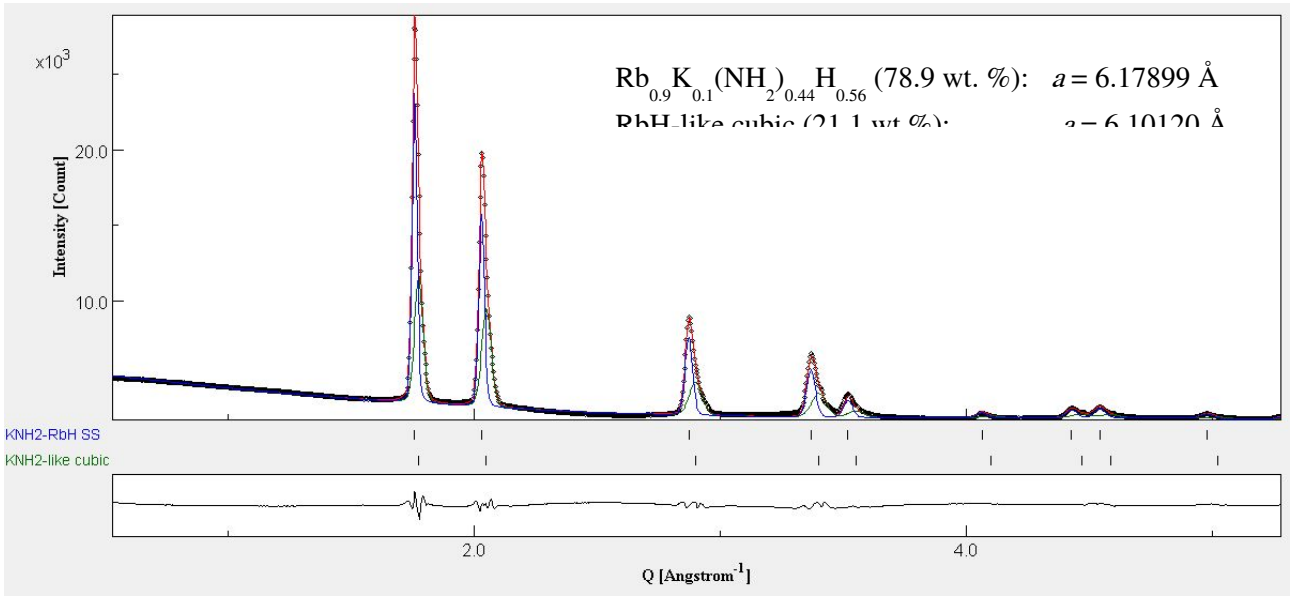

Figure S4. Rietveld refinement of *in-situ* SR-PXD data acquired at 270 ˚C for starting and mixed samples: (a) $RbNH_2$, (b) KH, (c) 0.7$RbNH_2$+0.3KH, (d) 0.5$RbNH_2$+0.5KH, (e) KNH_2, (f) RbH, (g) 0.7KNH_2+0.3RbH and (h) 0.5KNH_2+0.5RbH.

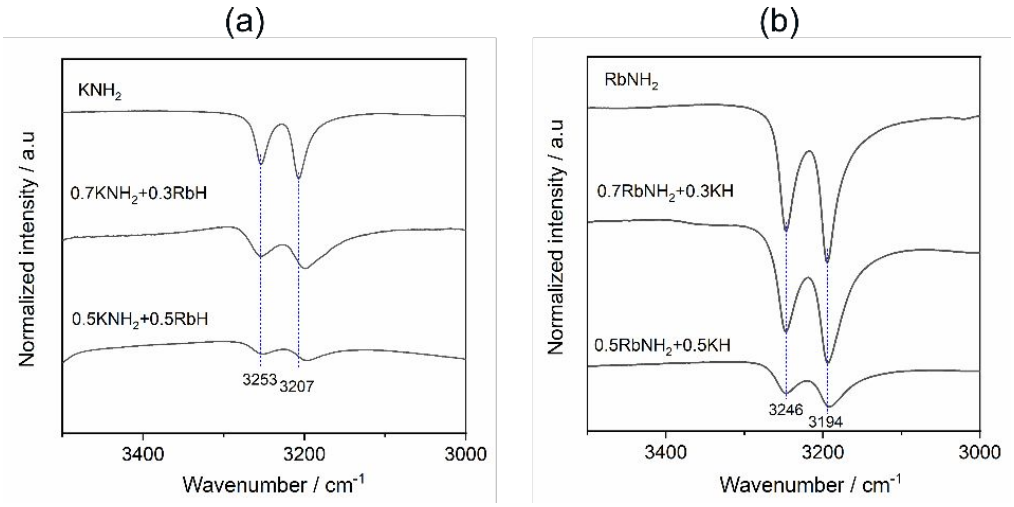

Figure S5. FT-IR of (a) $xKNH_2+(1–x)RbH$ and (b) $xRbNH_2+(1–x)KH$ samples.